Preprints of the 21st IFAC World Congress (Virtual)
Berlin, Germany, July 12-17, 2020

Reconfiguration Strategy for a Heavy Mobile Robot with Multiple Steering Configurations

Pushpendra Kumar * **Ismail Bensekrane** ** **Othman Lakhal** *** **Rochdi Merzouki** ***

* *Department of Mechanical Engineering, Graphic Era University, Dehradun, Uttarakhand, India (e-mail: jahan.pushp@gmail.com)*
** *Ecole Superieure Ali Chabati, Reghaia, Algiers, Algeria (e-mail: ismail.bensekrane@gmail.com)*
*** *Laboratory CRIStAL UMR CNRS 9189, Polytech Lille, University of Lille, 59655 Villeneuve d'Ascq, France, (e-mail: othman.lak@gmail.com; rochdi.merzouki@polytech-lille.fr)*

Abstract: A redundant robot can complete a given task even in a faulty situation using its alternative configurations. This paper presents a reconfiguration strategy for a redundant heavy mobile robot called Robutainer. It is a four wheeled mobile robot, which is used to transport 40 feet container in port terminals. Robutainer has redundant steering actuations for the front and rear sides, due to this redundancy, it shows four steering configurations namely, dual, front, rear, and skid. Thus, Robutainer can reconfigure between its four steering configurations when subjected to a fault in the steering system. But, it is necessary to detect and isolate a fault in the steering system; subsequently, the robot can be reconfigured according to the available steering configurations. The steering system of Robutainer is a complex multi-domain system with hybrid dynamics. In this work, a graphical modeling approach Bond Graph (BG) is used to develop the fault detection and isolation (FDI) model of the steering system considering its multi-domain components including electric motor, pump, accumulator, hydraulic motor, and transmission; moreover, discrete dynamics of distributor valves are included. Finally, a reconfiguration strategy is developed in order to reconfigure the system according to faults in the components of the steering system. The developed algorithm is verified through simulation in Matlab/Simulink with different components faults, and the experimental data of the robot tracking with four steering configurations is used to develop the reconfiguration strategy.

Keywords: Mobile robot, Dynamics, Bond graph, FDI, Reconfiguration.

1. INTRODUCTION

Wheeled mobile robots (WMRs) have increasingly been used in various ground maneuvering applications due to their design simplicity compared to legged and articulated robots. WMRs are mainly used in confined spaces such as manufacturing units, warehouses, port terminals, etc., for the purpose of transporting goods and people. Due to their autonomous operations, safety becomes the major concern. Therefore, it becomes necessary to detect and isolate faults in a system and to perform required reconfiguration, in order to avoid any accident. Generally, redundancy is used to improve the reliability of such systems (Catelani et al. (2017)).

The complex systems can have faults in their components and it becomes necessary to detect and isolate these faults, so that required action can be taken. Fault detection and isolation (FDI) methods include model-based and non model-based. Focusing on model-based methods (Cho et al. (2018)), they check the consistency between the actual process and its model using Analytical Redundancy Relations (ARRs). In this work, Bond Graph (BG) is used as a tool to develop the FDI model, because theory of FDI is well developed in BG (Merzouki et al. (2012)). BG has been used to develop FDI model of complex systems using diagnostic bond graph (DBG) (Kumar et al. (2014)). Moreover, BG has been applied successfully for diagnosis of hybrid systems having continuous and discrete dynamics simultaneously, using diagnostic hybrid bond graph (DHBG) as presented in Low et al. (2009). BG is a modular modeling tool that can be used to model a complex system systematically by considering its different multi-physics components. Focusing on mobile robots, many researchers rely on BG for dynamic modeling, control, and fault diagnosis of WMRs (Sahoo and Chiddarwar (2018),Termeche et al. (2018)). BG based fault recoverability analysis has been performed on a heavy mobile robot with continuous dynamics (Loureiro et al. (2012)). In Arogeti et al. (2012), BG based FDI has been performed for the hybrid steering system considering discrete and continuous dynamics.

In the existing works on FDI of WMRs, they generally focused on the one steering configuration of a robot, but due to redundancy of actuators, a robot can acquire multiple steering configurations. Therefore, in this work, a

reconfiguration strategy is developed for a heavy redundant mobile robot. An integrated approach using BG is developed for the modeling, FDI, and reconfiguration of the multi-domain hydro electromechanical steering system. The objective of this approach is to perform on-line reconfiguration of the robot when subjected to a fault, so that blocking of traffic and accidents can be avoided in the port terminals.

The remaining paper is organized in the following sections. The description of the considered mobile robot is given in Section 2. In Section 3, FDI model of the steering system is developed. Simulation results are discussed in Section 4. In Section 5, the reconfiguration strategy is developed for the robot. Finally, the paper is conclude in Section 6.

2. DESCRIPTION OF THE ROBOT

In this work, a heavy mobile robot with four traction wheels is considered, which is called Robutainer (Fig. 1). This heavy mobile robot is used to transport 40 feet container in port terminals. Robutainer have redundancy of actuations, where four independent DC motors are used to control the rotation of four traction wheels; in addition, there are two independent hydraulic motors to control the steering angles of the front and rear axles. The steering system is a hydro electromechanical system.

Fig. 1. Heavy redundant mobile robot, Robutainer.

Knowing that the robot moves in the port environment, the planar motion is sufficient to describe the dynamic behavior. In a plane, three degrees of freedom (DoF) are necessary i.e., motions in longitudinal, lateral, and yaw directions. Hence, three actuators are required to control motions in the three directions. But, Robutainer have four traction and two steering actuators, which represents an over-actuated system with six actuations to control three DoF. It is to be noted that internal DoF and actuators are not considered here. Therefore, degree of actuation redundancy (DoR) can be defined as the difference between total number of active actuations and number of DoF.

$$DoR = N - DoF \tag{1}$$

where, N represents the total number of input active actuators. Robutainer shows four configurations based on its two steering actuations as shown in Fig. 2.

In Fig. 2, four configurations are shown namely, dual, front, rear, and skid. Robutainer is assumed to be symmetric about its center of mass (CoM). The longitudinal and lateral directions of the robot are along the x and y axis, respectively. The yaw motion is along the axis perpendicular to the plane. In the front steering configuration, only the front side steering system is active, while the rear side is passive or faulty. In rear, only the rear

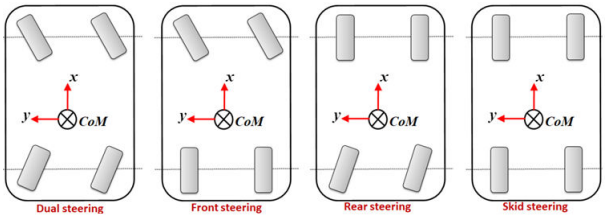

Fig. 2. Four steering configurations of Robutainer.

side steering system is active. In dual, both the steering systems are active. In the skid configuration, none of the steering system is active and the skid steering is performed using the traction wheels.

3. BG BASED FDI IN THE STEERING SYSTEM

The steering system of Robutainer is hydraulic, which consists of electric motor, pump, distributor valve, hydraulic motor, and transmission. The functional diagram of the system is shown in Fig. 3.

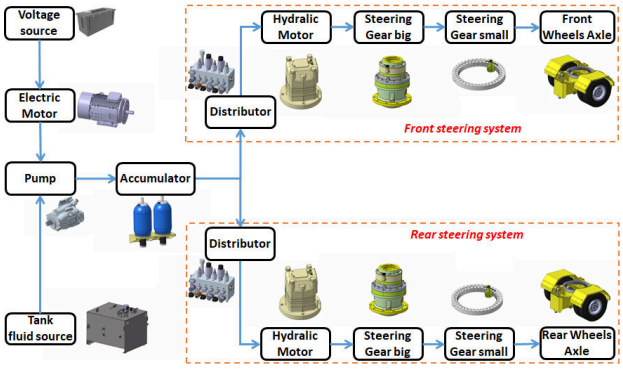

Fig. 3. Components of Robutainer's steering system.

In Fig. 3, the battery provides voltage to the electric motor which runs a hydraulic pump. The pump takes fluid (oil) from a source reservoir at atmospheric pressure i.e., tank, and transfer oil to an accumulator at high pressure. From the accumulator, the high pressure oil is distributed to the front and rear hydraulic motors via distributor valves. The rotations of hydraulic motors result in steering of the front and real axles through gears transmission. There are two gear pairs, first pair is having high gear ratio and the second pair is with low gear ratio. Therefore, the steering system of Robutainer is a complex system with multi-domain components. Furthermore, it becomes more complex due to discrete dynamics of the distributor valves due to opening and closing of valves' ports P, T, A, and B, which are shown in Fig. 4 (Kumar et al. (2019)).

Based on the above description of the steering system, it can be observed that it is a hybrid system representing the confluence of continuous and discrete dynamics. Thus, modeling of such complex system is challenging due to multi-domain nature and hybrid dynamics. BG has been proved a suitable tool to model multi-domain systems. Moreover, BG has been extended to model hybrid system called hybrid bond graph (HBG). Diagnostic HBG (DHBG) has been developed by solving the issue of causality change in HBG, and Global ARRs (GARRs) are proposed for the hybrid dynamical systems (Low et al.

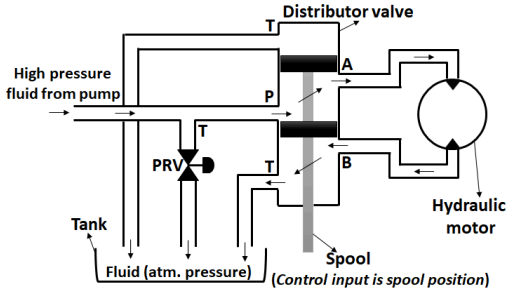

Fig. 4. Schematic of the distributor valve mechanism.

Table 1. Description of the discrete variables for different valves' modes.

Con.	V.M.	a_{1f}	a_{2f}	a_{3f}	a_{4f}	a_{5f}	a_{1r}	a_{2r}	a_{3r}	a_{4r}	a_{5r}	Di.
Front	M1	0	1	1	0	0	0	0	0	0	0	A
	M2	0	0	0	1	1	0	0	0	0	0	C
Rear	M3	0	0	0	0	0	0	1	1	0	0	A
	M4	0	0	0	0	0	0	0	0	1	1	C
Dual	M5	0	1	1	0	0	0	0	0	1	1	AF-CR
	M6	0	0	0	1	1	0	1	1	0	0	CF-AR
Skid	M7	1	0	0	0	0	1	0	0	0	0	N
	Con. – Configuration; **V.M.** – Valve modes; M1 – Mode1; and so on. **Di.** – Direction of steering; A – Anticlockwise; C – Clockwise; N – None; AF – Anticlockwise front; CR – Clockwise rear; CF – Clockwise front; AR – Anticlockwise rear.											

(2009), Wang et al. (2013)). For more details about BG, one may refer to Merzouki et al. (2012). In this paper, DHBG of the steering system is developed in order to perform FDI on it. Considering the different components in Fig. 3, the DHBG model of the steering system is shown in Fig. 5.

Refer to Fig. 5, DHBG is developed in derivative causality for each component of the system in line with Fig. 3. The input voltage U to electric motor is modeled using a source of effort (SE) element; similarly, other dynamics are modeled using BG elements including inertial (I), resistive (R), capacitative (C), transformer (TF), and gyrator (GY). The meaning of different parameters are given in Table 2. There are ten sensors in the system modeled with SSf and SSe, which represent signal sources. $\dot{\theta}_M$, $\dot{\delta}_f$, and $\dot{\delta}_r$ represent angular velocities of electric motor, front steering, and rear steering, respectively. P_P, P_{Vf}, P_{Af}, P_{Bf}, P_{Vr}, P_{Ar}, and P_{Br} represent pressure signals in accumulator, at the entry of front distributor valve, at A side of front hydraulic motor, at B side of front hydraulic motor, at the entry of rear distributor valve, at A side of rear hydraulic motor, at B side of rear hydraulic motor, respectively. Discrete modes of two distributor valves are modeled with controlled 1-junctions having discrete variables $a_{1f}, ...a_{5f}$ and $a_{1r}, ...a_{5r}$. State of these discrete variables are described in Table 1 for seven different valves' modes $M_1, ...M_7$. Note: the subscripts 'f' and 'r' denote parameters corresponding to front and rear steering systems, respectively.

The electric motor, pump, and accumulator are common components to both the front and rear; while distributor valve, hydraulic motor, and gears are separate for the front and rear systems. The signal sources (SSf and SSe) in DHBG represent sensors in the system; corresponding to these ten signal sources, ten GARRs can be derived from the DHBG. Considering the 1 junction corresponding to $\dot{\theta}_M$ sensor, GARR 1 is derived as follows:

$$GARR_1(\dot{\theta}_m) : \frac{K_m}{R_m}(U - K_m\dot{\theta}_m) - J_M\ddot{\theta}_m - f_M\dot{\theta}_m - V_P P_P = 0 \tag{2}$$

Similarly, other nine GARRs can be derived as described in Kumar et al. (2019). For robust diagnosis, parametric uncertainties are considered based on linear fractional transformation (LFT)-BG (Djeziri et al. (2007)). From LFT-BG, uncertain part of the $GARR_1$ represents adaptive threshold t_{h1} forming an envelope for residual R_1 ($-t_{h1} \leq R_1 \leq t_{h1}$).

$$t_{h1} = \left|\frac{K_{Mn}^2}{R_{Mn}} w_{K_{M2}}\right| + |K_{Mn} w_{K_{M1}}| - \left|K_{Mn} w_{1/R_M}\right| + |w_{J_M}| + |w_{f_M}| + |V_{Pn} w_{V_{P2}}| \tag{3}$$

The suffix n denotes nominal value of a parameter. $w_{K_{M2}}$, $w_{K_{M1}}$, w_{1/R_M}, w_{J_M}, w_{f_M}, and $w_{V_{P2}}$ represent uncertainties in respective parameters. Similarly, adaptive thresholds can be derived for the other nine GARRs. The FSM is developed by analyzing the ten GARRs, and it is presented in Table 2.

In Table 2, each component (electric motor, pump, accumulator, etc.) is composed of various parameters, and each parameter fault is sensitive to some residuals (R_1, R_2,...R_{10}). All components of the steering system have different rate and probability of malfunctions. In case of faults in valves' parameters, detectability and isolability depend on dynamic states of discrete variables (a_{1f}, a_{1r}...). The description of these discrete variables for different modes of valves is given in Table 1. It can be observed that all parameter faults are detectable (D_b), but some of the parameter faults are not isolable (I_b). In our analysis, we focus on faults at the component level and the fault isolability at the parameter level is ignored. Therefore, an extra column for the component isolability (I_{bc}) is added to FSM, in which, it can be seen that all the components faults are isolable, and the effect of a component fault on front, rear, or both systems is specified.

4. SIMULATION RESULTS

Presently, it is not possible to provoke faults in Robutainer due to safety reasons. Therefore, the developed FDI model is simulated in Matlab/Simulink in order to verify the algorithm. The numerical values of different parameters are given in Table 2, which are estimated based on the technical specifications provides by the manufacturer of different components. To evaluate adaptive thresholds, the uncertainties in parameters' values are kept less than ten percent. The objective of simulation is to analyze the performance of the steering system in case of faults in its components; consequently, Robutainer can reconfigure to an available steering configuration (Fig. 9). It is assumed that Robutainer can switch between its redundant steering configurations.

4.1 First scenario: constant mode of valves

In this scenario, valves' mode is kept constant i.e., state of discrete variables is not changing with respect to time. The performance of the FDI model is analyzed in fifth mode M5 i.e., anticlockwise front and clockwise rear steering (Table 1). The following cases are considered in this scenario a)

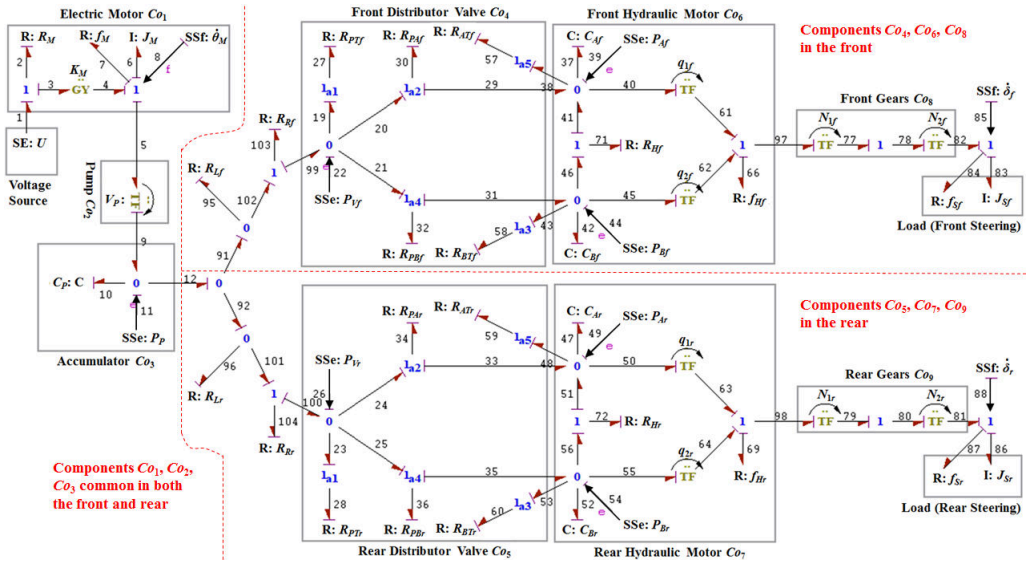

Fig. 5. Diagnostic hybrid bond graph (DHBG) of the steering system of Robutainer.

no fault, b) fault in electric motor, and c) fault in front valve. The results are shown in Fig. 6.

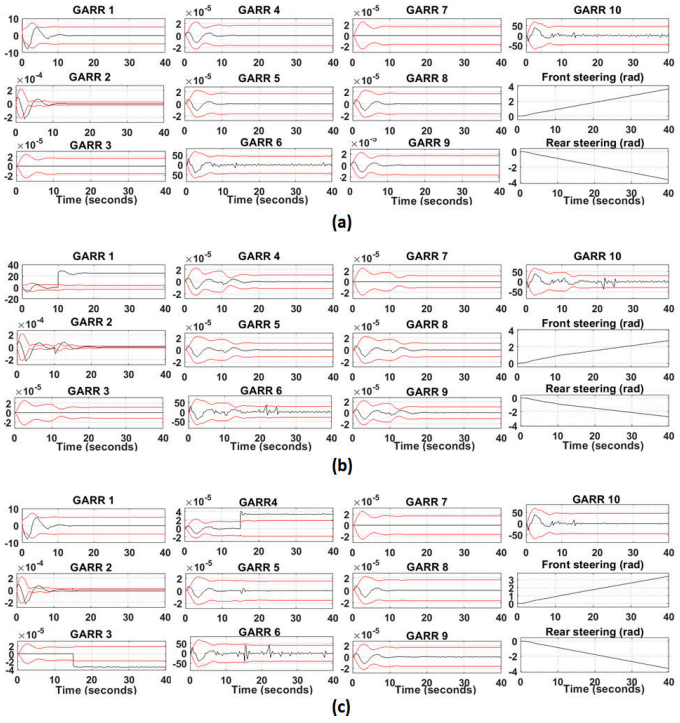

Fig. 6. First scenario of constant valves mode, results showing ten GARRs and steering angles, thresholds in red curves (a) no fault, (b) fault in electric motor, and (c) fault in front valve.

In Fig. 6 (a), the first case is simulated considering all the components are healthy, it can be observed that all residuals (black curves) are within the thresholds (red curves), which represents no fault situation and verifies the FDI algorithm. In this ideal healthy situation, both the front and rear steering angles reach to 3.64 rad in 40 s. Since, no fault in the system, all the steering configurations are available to use, i.e., dual, front, rear, and skid.

In Fig. 6 (b), the second case is simulated considering fault in the electric motor i.e., resistance of motor is increased by 50 percent after 10 s. It can be seen that only residual 1 (GARR 1) is out of threshold, refer to Table 2, residual-1 is sensitive to fault in electric motor, which is common to both the front and rear systems. Due to this fault, the steering angles attain a value of 2.74 rad in 40 s, which is lesser compared to 3.64 rad in the healthy situation. Since, this fault is common to both the front and rear systems, the only available configuration is skid.

In Fig. 6 (c), the third case is simulated considering fault in the front distributor valve; ports of the valve are chocked i.e., resistance to flow from port P to A (Fig. 4) is increased by 20 percent after 15 seconds. It can be observed that residuals 3 and 4 are out of threshold, refer to Table 2, combination of residuals 3 and 4 is sensitive to fault in front valve. Due to this fault, the performance of front steering reduces and the angle reaches to only 3.44 rad in 40 s. Since, this fault affects the front system, the available configurations are rear and skid.

4.2 Second scenario: changing mode of valves

In this scenario, valves mode is changing rapidly: M7 till 10 seconds, M5 till 14 seconds, M7 till 16 seconds, M6 till 20 seconds, and M7 after 20 seconds. Therefore, four times mode changes in a period of ten seconds (Table 1). The following cases are considered in this scenario a) no fault, b) fault in electric motor, and c) fault in rear hydraulic motor. The results are shown in Fig. 7.

In Fig. 7 (a), the first case is simulated considering all the components are healthy, it can be observed that there are many peaks of residuals which do not respect thresholds, since there are rapid changes in valves modes between 10 to 20 s. However, these peaks are temporary and disappear after the transition period (10 to 20 s), which represents healthy situation. In this ideal healthy situation, both the front and rear steering angles reach to maximum value of 0.38 rad at 14 s. Here, all the configurations are available. In Fig. 7 (b), the second case is simulated considering fault

Table 2. FSM for the steering system of Robutainer.

Co.	Parameters	R_1	R_2	R_3	R_4	R_5	R_6	R_7	R_8	R_9	R_{10}	D_b	I_b	I_{bc}
Electric Motor	R_M Motor resistance (1.5 Ω)	1										1	0	1
	K_M Mot. constant (0.3 Nm/A)	1										1	0	Common
	J_M Motor inductance (0.6 H)	1										1	0	
	f_M Motor Friction (0.21 N-m-s/rad)	1										1	0	
Pump	V_P Pump constant (1.761e-5 m^3/rad)	1	1									1	1	1
Accumu. & Pipelines	C_P Accumulator compliance (2.1739e9 Pa/m^3)		1									1	0	Com 1
	R_{Lf} Leakage in front pipeline (1e30 Pa-s/m^3)		1									1	0	Common
	R_{Lr} Leakage in rear pipeline (1e30 Pa-s/m^3)		1									1	0	
Front Distributor Valve	R_{PTf} Front valve resistance for port P to T (1e10 Pa-s/m^3)			a_{1f}								a_{1f}	a_{1f}	1
	R_{PAf} Front valve resistance for port P to A (1e10 Pa-s/m^3)			a_{2f}	a_{2f}							a_{2f}	a_{2f}	
	R_{PBf} Front valve resistance for port P to B (1e10 Pa-s/m^3)			a_{4f}		a_{4f}						a_{4f}	a_{4f}	
	R_{ATf} Front valve resistance for port A to T (1e10 Pa-s/m^3)				a_{5f}							a_{5f}	a_{5f}	
	R_{BTf} Front valve resistance for port B to T (1e10 Pa-s/m^3)					a_{3f}						a_{3f}	a_{3f}	Front
Rear Distributor Valve	R_{PTr} Rear valve resistance for port P to T (1e10 Pa-s/m^3)							a_{1r}				a_{1r}	a_{1r}	1
	R_{PAr} Rear valve resistance for port P to A (1e10 Pa-s/m^3)							a_{2r}	a_{2r}			a_{2r}	a_{2r}	
	R_{PBr} Rear valve resistance for port P to B (1e10 Pa-s/m^3)							a_{4r}		a_{4r}		a_{4r}	a_{4r}	
	R_{ATr} Rear valve resistance for port A to T (1e10 Pa-s/m^3)								a_{5r}			a_{5r}	a_{5r}	
	R_{BTr} Rear valve resistance for port B to T (1e10 Pa-s/m^3)									a_{3r}		a_{3r}	a_{3r}	Rear
Front Hydraulic Motor	R_{Hf} Internal leakage in front hydraulic mot. (1e30 Pa-s/m^3)				1	1						1	1	1
	q_{1f} Front hydraulic motor displacement for A side (6.2893e4 rad/m^3)				1		1					1	1	
	q_{2f} Front hydraulic motor displacement for B side (-6.2893e4 rad/m^3)					1	1					1	1	
	f_{Hf} Front hydraulic motor friction (0.37 N-m-s/rad)						1					1	1	Front
Rear Hydraulic Motor	R_{Hr} Internal leakage in rear hydraulic mot. (1e30 Pa-s/m^3)								1	1		1	1	1
	q_{1r} Rear hydraulic motor displacement for A side (6.2893e4 rad/m^3)								1		1	1	1	
	q_{2r} Rear hydraulic motor displacement for B side (-6.2893e4 rad/m^3)									1	1	1	1	
	f_{Hr} Rear hydraulic motor friction (0.37 N-m-s/rad)										1	1	1	Rear
Front Gears	N_{1f} Front big gear ratio (0.04807)				1	1	1					1	1	1
	N_{2f} Front small gear ratio (0.16666)				1	1	1					1	1	Front
Rear Gears	N_{1r} Rear big gear ratio (0.04807)								1	1	1	1	1	1
	N_{2r} Rear small gear ratio (0.16666)								1	1	1	1	1	Rear

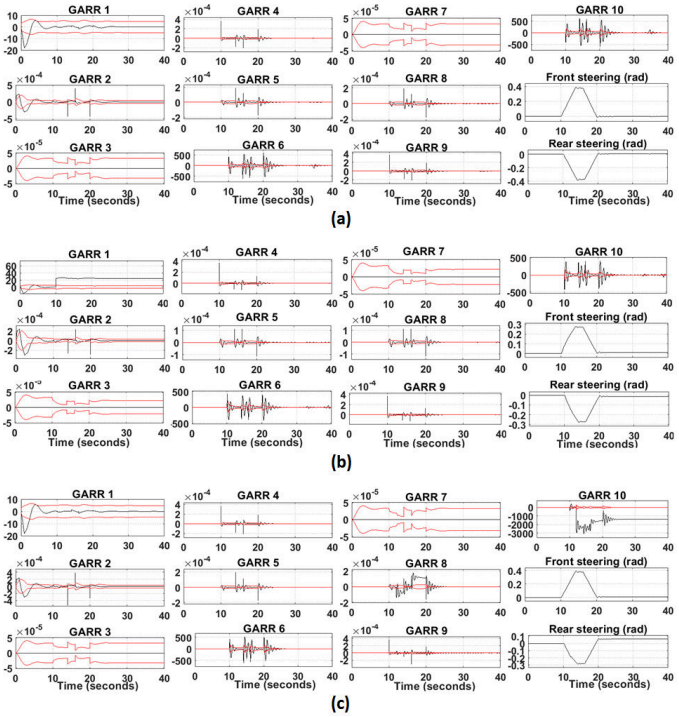

Fig. 7. Second scenario of changing valves mode, results showing ten GARRs and steering angles, thresholds in red curves (a) no fault, (b) fault in electric motor, and (c) fault in rear hydraulic motor.

in the electric motor; resistance of motor is increased by 50 percent after 10 s. It can be seen that only GARR 1 is permanently out of threshold, which represents the fault in electric motor. Due to this fault, the steering angles attain a maximum value of 0.27 rad at 14 s, which is lesser compared to 0.38 rad in the healthy situation. Since, electric motor is a common component to both the front and rear systems, the only available configuration is skid.

In Fig. 6 (c), the third case is simulated considering fault in the rear hydraulic motor; the motor displacement q_{1r} is decreased by 40 percent after 12 seconds. It can be observed that GARR 8 and 10 are showing significant disturbed behavior after 12 seconds, refer to Table 2, the combination of residuals 8 and 10 is sensitive to fault in rear hydraulic motor. Due to this fault, the performance of rear steering reduces and the angle reaches to only 0.28 rad at 14 s. Since, this fault is in rear system, the available configurations are front and skid.

Based on the above results, it can be concluded that the developed FDI algorithm performs well for this complex multi-domain and hybrid steering system. In the following section, a reconfiguration strategy is developed, which suggest that which configuration should be used among all the available configurations, when subjected to a fault.

5. RECONFIGURATION STRATEGY

Based on this fault diagnosis, the system can be reconfigured to an alternative available steering configuration, in order to complete a given task and to avoid the safety risks. Experiments on Robutainer have been performed to analyze the performance of trajectory tracking with different steering configurations (Fig. 8).

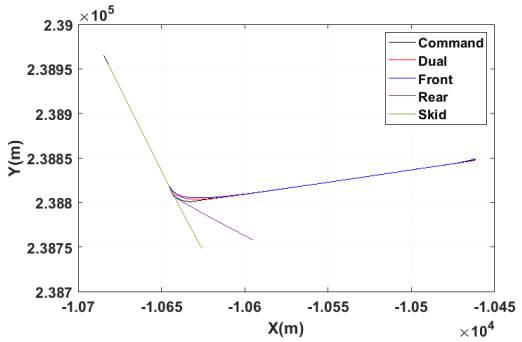

Fig. 8. Trajectory tracking with different configurations.

From Fig. 8, it can be observed that the robot can track the command trajectory using all the four configurations when there are straight path and smooth curves. But, the robot is unable to track a sharp turn using rear and skid configurations. Moreover, the dual configuration tracks the sharp turn better than the front configuration. Based on these observations, the developed reconfiguration strategy is presented in Fig. 9.

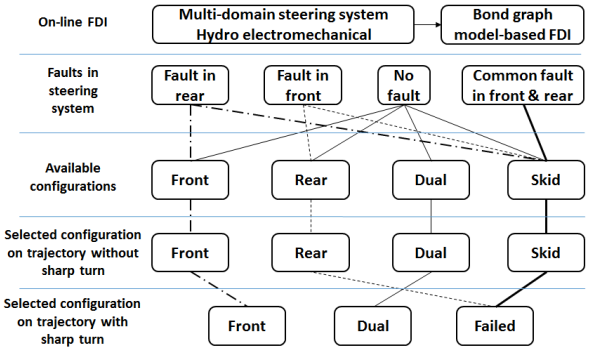

Fig. 9. Reconfiguration strategy.

Refer to Fig. 9, two types of trajectories are considered i.e., without sharp turn and with sharp turn. Based on the observations from the experimental results, the four configurations can be prioritize as follows: $dual > front > rear > skid$. When a fault is isolated in the rear steering system, then the front and skid configurations will be available to complete the task, and according to priority front will be selected which can track a trajectory with and without sharp turns. In case of faulty front steering system, the available configurations are rear and skid, the rear configuration will be selected, but only for a trajectory without sharp turns, the system will be failed on a trajectory with sharp turns. If there is no fault, the robot will track with dual because it is the best configuration to track trajectory with and without sharp turns. When a fault is isolated in a component which is common to both the front and rear steering systems, then the only available configuration is skid, which represents a failed system when tracking a sharp turn. Based on this strategy, the selected configurations for the different steering faults simulated in Fig. 6 and 7 can be suggested.

6. CONCLUSION

In the present work, a heavy mobile robot is analyzed for its steering configurations, and a reconfiguration strategy is developed using experimental data of the robot. Due to redundant steering actuations, this mobile robot can have four steering configurations namely, dual, front, rear, and skid. It can reconfigure to any available steering configuration when subjected to a fault. Hence, FDI becomes necessary to detect and isolate a fault in the steering system, so that an available steering configuration can be identified. The developed FDI model is verified through simulation and results show satisfactory performance of the algorithm. For future work, it is interesting to consider more configurations of the robot considering active and passive traction actuators.

REFERENCES

Arogeti, S.A., Wang, D., Low, C.B., and Yu, M. (2012). Fault detection isolation and estimation in a vehicle steering system. *IEEE Transactions on Industrial Electronics*, 59(12), 4810–4820.

Catelani, M., Ciani, L., Patrizi, G., and Venzi, M. (2017). Reliability allocation procedures in complex redundant systems. *IEEE Systems Journal*, 12(2), 1182–1192.

Cho, S., Gao, Z., and Moan, T. (2018). Model-based fault detection, fault isolation and fault-tolerant control of a blade pitch system in floating wind turbines. *Renewable energy*, 120, 306–321.

Djeziri, M.A., Merzouki, R., Bouamama, B.O., and Dauphin-Tanguy, G. (2007). Robust fault diagnosis by using bond graph approach. *IEEE/ASME Transactions on Mechatronics*, 12(6), 599–611.

Kumar, P., Bensekrane, I., Conrard, B., Toguyeni, A., and Merzouki, R. (2019). Functionability analysis of redundant mechatronics systems in bond graph framework. *IEEE/ASME Transactions on Mechatronics*, 24(6), 2465–2476.

Kumar, P., Merzouki, R., Conrard, B., and Bouamama, B.O. (2014). Multilevel reconfiguration strategy for the system of systems engineering: Application to platoon of vehicles. *Proceedings of the 19th World Congress, The International Federation of Automatic Control (IFAC 2014) Cape Town, South Africa*, 8103–8109.

Loureiro, R., Merzouki, R., and Bouamama, B.O. (2012). Bond graph model based on structural diagnosability and recoverability analysis: Application to intelligent autonomous vehicles. *IEEE Transactions on Vehicular Technology*, 61(3), 986–997.

Low, C.B., Wang, D., Arogeti, S., and Luo, M. (2009). Quantitative hybrid bond graph-based fault detection and isolation. *IEEE Transactions on Automation science and engineering*, 7(3), 558–569.

Merzouki, R., Samantaray, A.K., Pathak, P.M., and Bouamama, B.O. (2012). *Intelligent mechatronic systems: modeling, control and diagnosis*. Springer Science & Business Media.

Sahoo, S.R. and Chiddarwar, S.S. (2018). Mobile robot control using bond graph and flatness based approach. *Procedia computer science*, 133, 213–221.

Termeche, A., Benazzouz, D., Bouamama, B.O., and Abdallah, I. (2018). Augmented analytical redundancy relations to improve the fault isolation. *Mechatronics*, 55, 129–140.

Wang, D., Yu, M., Low, C.B., and Arogeti, S. (2013). *Model-based health monitoring of hybrid systems*. Springer.